This article has been accepted for inclusion in a future issue of this journal. Content is final as presented, with the exception of pagination.

Per-Phase Stator-Resistance Estimation by DC-Signal Injection in Open-Phase Fault-Tolerant Six-Phase Induction Motor Drives

Alejandro G. Yepes, *Senior Member, IEEE*, Mahmoud Said Abdel-Majeed, Wessam E. Abdel-Azim, Mohamed G. Abdel-Moneim, Ayman Samy Abdel-Khalik, *Senior Member, IEEE*, Shehab Ahmed, *Senior Member, IEEE*, and Jesús Doval-Gandoy, *Member, IEEE*

***Abstract*—Multiphase machine drives are advantageous over three-phase ones in features such as tolerance to open-phase faults (OPFs). Six-phase (6P) ones offer an excellent compromise between complexity and fault tolerance. In particular, those with a symmetrical arrangement of the stator phase windings and a single neutral point provide superior postfault capability. To ensure high reliability and performance, the stator resistance should be monitored. This can be attained with good robustness to uncertainties by dc-signal injection. This article proposes a dc-based resistance estimation method for symmetrical 6P induction machines that achieves the following main characteristics simultaneously for the first time: estimation of individual stator phase resistances and suitability for either healthy or OPF conditions. The dc injection is performed so that no torque ripple is produced and so that the increase in loss, peak current, and braking torque is relatively small. The method is designed so that it is robust to the deviation in the stator neutral-point voltage due to resistance asymmetry. Experimental results are provided.**

***Index Terms*—Fault tolerance, multiphase drives, signal injection, six-phase (6P) machine, stator resistance, variable-speed drives.**

Manuscript received 18 March 2024; revised 16 May 2024; accepted 9 June 2024. This work was supported in part by MCIN/AEI/10.13039/501100011033 and by the European Union ≪NextGenerationEU≫ /PRTR under Project CNS2022-135773, in part by the Government of Galicia under Grant ED431F 2020/07 and Grant GPC-ED431B 2023/12, in part by the Ministry of Science, Innovation and Universities under the Ramon y Cajal under Grant RYC2018-024407-I, and in part by MCIU/AEI/10.13039/501100011033/FEDER-UE under Project PID2022-136908OB-I00, and in part funding for open access charge by Universidade de Vigo/ CRUE-CISUG. *(Corresponding author: Jesús Doval-Gandoy.)*

Alejandro G. Yepes and Jesús Doval-Gandoy are with Applied Power Electronics Technology (APET) Research Group, CINTECX, Universidade de Vigo, 36310 Vigo, Spain (e-mail: agyepes@uvigo.es; jdoval@uvigo.es).

Mahmoud Said Abdel-Majeed, Wessam E. Abdel-Azim, Mohamed G. Abdel-Moneim, and Ayman Samy Abdel-Khalik are with the Electrical Engineering Department, Faculty of Engineering, Alexandria University, Alexandria 21544, Egypt (e-mail: es-mahmoud.said1415@alexu.edu.eg; wessam.essam@alexu.edu.eg; mohamed.g.abdelmoneim@alexu.edu.eg; ayman.abdel-khalik@alexu.edu.eg).

Shehab Ahmed is with CEMSE Division, King Abdullah University of Science and Technology, Thuwal 23955, Saudi Arabia (e-mail: shehab.ahmed@kaust.edu.sa).

This article has supplementary material provided by the authors and color versions of one or more figures available at https://doi.org/10.1109/TIE.2024.3417992.

Digital Object Identifier 10.1109/TIE.2024.3417992

I. INTRODUCTION

MULTIPHASE machine drives are receiving considerable attention due to their advantages compared with three-phase ones [1]. Some of the main benefits are reduced phase-current rating and dc-link capacitors [2], lower torque ripple [3], and most importantly, enhanced fault tolerance [1], [4]. Accordingly, n-phase ($n > 3$) drives are especially attractive for applications where high reliability is sought (even for low power), such as aerospace vehicles and remote wind-energy farms [1], [4]. In particular, open-phase faults (OPFs) are one of the most common failures tolerated by these drives [4], [5], [6]. OPFs can be caused by an open-circuit fault in the stator windings/connections or by isolating certain elements (e.g., converter legs) where a problem (e.g., short circuit) has arisen [1], [6], [7], [8]. Among the various types of multiphase drives, six-phase (6P) ones are very popular due to, e.g., their moderate complexity (increasing with n) and suitability for off-the-shelf three-phase converters [2], [4]. In addition, although the achievable torque under OPF rises with n, that corresponding to $n = 6$ is already relatively high ([8], Fig. 5). Among 6P machines, those with symmetrical winding arrangement and a single neutral point are preferred from the viewpoint of postfault torque capability [6], control simplicity, and (especially for small winding space harmonics) current distortion [9].

Another crucial aspect for ensuring high reliability and performance is monitoring the resistance of the stator phase windings and of elements in series with them such as cables and connectors (henceforth, collectively called stator resistance for simplicity), for various reasons. Its value can be employed to detect faults such as high-resistance connections (due to vibration, oxidation, etc. [10], [11]) before they degrade to more serious problems [10], [12]. Furthermore, the stator resistance may be used to estimate the machine temperature online so that overheating is avoided [13], [14], e.g., in case of abnormal cooling [15]. Alternatively, the variation of the stator resistance may be taken into account to adapt the drive

This article has been accepted for inclusion in a future issue of this journal. Content is final as presented, with the exception of pagination.

control parameters to attain better behavior, e.g., when using control types sensitive to its value such as model-predictive or direct-torque control [12], or when maximizing the efficiency through optimum current references under resistance asymmetry [11].

In any of these cases, the stator resistance may be obtained based on ac [16] or dc [12], [14], [15], [17] voltages and currents. The latter approach (dc) is much less affected by other aspects whose effects increase with frequency, such as skin effect, flux, back-electromotive force, inductances, and core loss [13], [15], [17]. In three-phase drives, where current can only flow in the $\alpha\beta$ plane, the dc injection tends to cause braking torque [18] and torque ripple [13], [14], [15]. This ripple may be alleviated by suitable injection of second-order harmonic [19], [20], but the machine model uncertainty may prevent its complete cancellation [17]. In contrast, the dc signals can be added in the nontorque-producing xy planes of multiphase machines (assuming insignificant space-harmonic effects) while avoiding the torque-producing $\alpha\beta$ plane, thus providing negligible torque disturbance [12], [14], [17].

A summary of the existing techniques based on dc-signal injection for multiphase machines is displayed in Table I. The first attempt of this kind was presented in [14], where the overall resistance of a healthy 6P stator winding was monitored. Unfortunately, it is not suitable for situations with resistance imbalance, which may occur due to problems such as high-resistance connections [10], [11], [12] and partial overheating [12], [21]. Conversely, the solution from [12] is able to find the stator resistance of each phase individually. However, these methods [12], [14] relied on extra physical devices for phase-voltage measurements, which are not commonly available in motor drives [15]. Moreover, most importantly, OPFs were not considered [12], [14], in spite of the importance of the OPF-tolerant operation [1], [4]. Their adaptation to OPFs is far from straightforward due to the coupling between the machine subspaces introduced by the faults [17]. The approach from [14] was extended to symmetrical 6P induction motors under a single OPF in [17]. The dc injection was modified to minimize the stator copper loss (SCL), peak current, and braking torque produced by the zero sequence (coupled with the xy plane) in the postfault situation. No extra devices were needed, thanks to the well-established output-voltage estimation [15] from the voltage references. Nonetheless, in [17], only the overall resistance was estimated, assuming all the per-phase resistances were identical, which, as aforesaid, is often untrue [12]. Actually, the resistance asymmetry caused by nonuniform temperature distribution is aggravated under OPFs. This is a consequence of the absence of current in some phases [22], [23] and of the fact that the current ac references should then be unbalanced to minimize the SCL [24]. Hence, a dc-injection method to monitor the stator resistance per phase under OPFs should be developed. Furthermore, given that an OPF in a single phase is the most likely OPF scenario [25], it should preferably be considered.

This article proposes a technique (Table I) based on dc-signal injection for estimating the stator resistance of each phase of a 6P machine with symmetrical winding arrangement and a single

TABLE I
REFERENCES ABOUT DC-SIGNAL INJECTION FOR RESISTANCE ESTIMATION IN MULTIPHASE DRIVES

References	Per-Phase Resistance	Healthy	OPFs
[14]	×	✓	×
[12]	✓	✓	×
[17]	×	×[†]	✓
This article	✓	✓	✓

Note: [†]Only OPF case is considered in [17], but it may be applied to healthy case.

neutral point, either in healthy or OPF conditions. The method is suitable for resistance imbalance. No extra devices for voltage measurement are necessary. The dc components are distributed among the phases so as to ensure relatively low torque disturbance, SCL, and peak currents. Experimental verification is carried out. In accordance with Table I, the main contributions with respect to [12] and [17] are the validity for OPFs and resistance asymmetry, respectively.

The rest of the article is organized as follows. The theoretical background is presented in Section II. The proposed resistance estimation for healthy and OPF conditions is explained in Sections III and IV, respectively. The experimental results are discussed in Section V. Finally, the conclusions are summarized in Section VI.

II. BACKGROUND

A. Vector Space Decomposition (VSD)

In a 6P machine with symmetrical windings (two three-phase sets displaced by $\gamma = 60^\circ$), a variable u (voltage v or current i) in phase coordinates may be expressed with respect to the VSD subspaces as [1], [17]

$$\underbrace{\big[\overbrace{u_\alpha \;\, u_\beta}^{\boldsymbol{u}_{\alpha\beta}} \;\, \overbrace{u_x \;\, u_y}^{\boldsymbol{u}_{xy}} \;\, u_{0^+} \;\, u_{0^-}\big]^{\mathrm{T}}}_{\boldsymbol{u}_{\mathrm{vsd}}} = \boldsymbol{D}\,\underbrace{\big[u_{\mathrm{a}} \;\, u_{\mathrm{b}} \;\, u_{\mathrm{c}} \;\, u_{\mathrm{d}} \;\, u_{\mathrm{e}} \;\, u_{\mathrm{f}}\big]^{\mathrm{T}}}_{\boldsymbol{u}_{\mathrm{ph}}} \quad (1)$$

$$\boldsymbol{D} = \frac{1}{3}\begin{bmatrix} 1 & \cos(\gamma) & \cos(2\gamma) & \cos(3\gamma) & \cos(4\gamma) & \cos(5\gamma) \\ 0 & \sin(\gamma) & \sin(2\gamma) & \sin(3\gamma) & \sin(4\gamma) & \sin(5\gamma) \\ 1 & \cos(2\gamma) & \cos(4\gamma) & \cos(6\gamma) & \cos(8\gamma) & \cos(10\gamma) \\ 0 & \sin(2\gamma) & \sin(4\gamma) & \sin(6\gamma) & \sin(8\gamma) & \sin(10\gamma) \\ 1/2 & 1/2 & 1/2 & 1/2 & 1/2 & 1/2 \\ 1/2 & -1/2 & 1/2 & -1/2 & 1/2 & -1/2 \end{bmatrix}. \quad (2)$$

The fundamental and third-order (if any) airgap flux components are associated with the $\alpha\beta$ plane and the 0^- axis, respectively [1], [26]. The torque production is mainly due to the former subspace [26]. Assuming that the windings are not chorded, the even space harmonics, corresponding to the xy plane, can usually be neglected [26]. It is also assumed that there is a single stator neutral point, formed by the connection (for better OPF performance [6]) of both three-phase neutral points, and that it is electrically isolated from the converter;

hence $i_{0+} = 0$, even if v_{0+} or the stator neutral-point voltage is not zero.

B. Generation of Current References for DC Injection

For any dc injection, the dc (denoted by overbar) injected current references may be generated using a system of six equations, expressed in matrix form as [17]

$$\boldsymbol{A}\bar{\boldsymbol{i}}_{\text{vsd}} = \boldsymbol{A}\begin{bmatrix}\bar{i}_\alpha & \bar{i}_\beta & \bar{i}_x & \bar{i}_y & \bar{i}_{0+} & \bar{i}_{0-}\end{bmatrix}^{\mathrm{T}} = \boldsymbol{B} \tag{3}$$

where $\boldsymbol{A}$ and $\boldsymbol{B}$ are 6×6 and 6×1 arrays, respectively, used to impose six constraints. If there are no OPFs, they are as follows:

$$\boldsymbol{A} = \begin{bmatrix}0&0&1&0&0&0\\0&0&0&1&0&0\\1&0&0&0&0&0\\0&1&0&0&0&0\\0&0&0&0&1&0\\0&0&0&0&0&1\end{bmatrix};\quad \boldsymbol{B} = \begin{bmatrix}I_{\text{dc}}\cos\phi\\I_{\text{dc}}\sin\phi\\0\\0\\0\\0\end{bmatrix}. \tag{4}$$

The first two rows mean that the dc current is injected in the xy plane with magnitude I_{dc} and angle ϕ [14], [17]. The third and fourth rows force the $\alpha\beta$ dc current to zero to avoid torque disturbance [14]. The fifth row corresponds to $\bar{i}_{0+} = 0$, which, as aforesaid, follows from the fact that the neutral point is isolated. In the sixth row, $\bar{i}_{0-}$ is set to zero to avoid extra SCL as well as braking torque associated with the third-order space harmonic [17]. In case of an OPF in the kth phase, the last row of $\boldsymbol{A}$ in (4) is replaced by the kth row of $\boldsymbol{D}^{-1}$ to include the current restriction introduced by the fault [17].

Then, from (3) and (1), the dc VSD and phase currents for either healthy or OPF conditions can be found as [17]

$$\bar{\boldsymbol{i}}_{\text{vsd}} = \begin{bmatrix}\bar{i}_\alpha & \bar{i}_\beta & \bar{i}_x & \bar{i}_y & \bar{i}_{0+} & \bar{i}_{0-}\end{bmatrix}^{\mathrm{T}} = \boldsymbol{A}^{-1}\boldsymbol{B} \tag{5}$$

$$\bar{\boldsymbol{i}}_{\text{ph}} = \begin{bmatrix}\bar{i}_{\text{a}} & \bar{i}_{\text{b}} & \bar{i}_{\text{c}} & \bar{i}_{\text{d}} & \bar{i}_{\text{e}} & \bar{i}_{\text{f}}\end{bmatrix}^{\mathrm{T}} = \boldsymbol{D}^{-1}\boldsymbol{A}^{-1}\boldsymbol{B}. \tag{6}$$

C. Current Control Scheme

Fig. 1 depicts a current control scheme suitable for driving a fault-tolerant induction machine with field-oriented control and dc injection. The references are indicated by an asterisk (dropped in other parts of the article for simplicity).

The ac and dc parts are denoted by $\tilde{}$ and $\bar{}$, respectively. The $\alpha\beta$ fundamental current reference $\tilde{\boldsymbol{i}}^*_{\alpha\beta}$, only containing positive sequence, is set based on the target flux and torque [27]. The ac components of $\tilde{\boldsymbol{i}}^*_{\text{vsd}}$ in the other VSD subspaces (with positive and negative sequences) are usually set in healthy case to zero and under OPF by the so-called minimum-loss (ML), maximum-torque (MT), or full-torque-range ML (FRML) strategies [8], [28]. The ML, MT, and FRML ac current references pursue minimum SCL, maximum-torque range, or both features simultaneously, respectively, while preserving ripple-free torque [8], [28]. If the resistance imbalance is notable, the enhanced FRML ac reference generation from [11] may be adopted to further reduce the ac SCL, either in healthy or OPF scenarios. On the other hand, the dc reference $\bar{\boldsymbol{i}}^*_{\text{vsd}}$ for the resistance estimation is obtained from (5).

The current error $\boldsymbol{e}_{\text{vsd}} = \boldsymbol{i}^*_{\text{vsd}} - \boldsymbol{i}_{\text{vsd}}$ is fed into a proportional-integral-resonant (PIR) controller in each VSD subspace, with the resonant and integral parts being responsible for the ac and dc tracking, respectively [17]. The resonant control, thanks to its ability to control both positive and negative sequences, is able to cancel the ac negative sequence in the $\alpha\beta$ current and to track the xy and 0^- ac current references even if they are set unbalanced (based on ML, MT, or FRML) due to OPFs or resistance asymmetry [1], [8], [11]. Although in healthy case, the ac and dc current references are only nonzero in the $\alpha\beta$ and xy planes, respectively, resonant and integral terms are also required in the other subspaces to reject the ac and dc disturbances due to any resistance asymmetry [10]. These aspects of the current control also help to compensate for the torque ripple and losses that resistance imbalance tends to cause [1], [8], [10]. An active resistance (increasing disturbance rejection) [29] may be added to the $\alpha\beta$ plane to help mitigate brief transient torque oscillations due to temporary $\alpha\beta$ dc current when the xy and 0^- dc current references change. Under an OPF, the 0^- axis is left uncontrolled in agreement with the fact that one degree of freedom is lost [30]. The output pole-voltage references $\boldsymbol{v}^*_{\text{p}}$ are synthesized by pulsewidth modulation (PWM) and may be used to estimate the phase resistances R_k, as explained shortly.

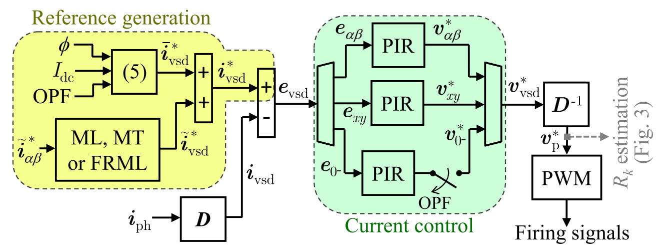

Fig. 1. Current control scheme to use with the proposed estimation method.

III. DC Injection and R_k Estimation in Healthy Case

Fig. 2 shows the dc VSD and phase currents as a function of ϕ obtained using (5) and (6), normalized by I_{dc}, when no OPFs exist. From Fig. 2(a), there is only dc current in the xy plane, as expected, avoiding torque disturbances. Since $\bar{i}_{0-} = 0$, the 0^- current does not cause braking torque or extra SCL [17]. In fact, if the stator resistance R asymmetry is neglected, the SCL is the same regardless of ϕ: $3I^2_{\text{dc}}R$. From Fig. 2(b), three dc phase currents $\bar{i}_k$ are equal to the other three, pairwise. When ϕ is a multiple of 60°, four $\bar{i}_k$ coincide at ±0.5 p.u., while the other two are ±1 p.u. Three of these ϕ values (0°, 120°, and 240°) are denoted in Fig. 2 as ϕ^ρ, with $\rho = 0, 1$, or 2. These three angles are selected for the proposed method because the phase-current magnitudes are relatively large, which is convenient for ensuring accuracy [12]. The peak phase current is increased by up to 1 p.u. by the dc injection, which needs to be taken into account, e.g., to avoid converter overcurrent [17]. Since ordinarily the resistance variations due to temperature or high-resistance connections are slow [10], [15] and no urgent actions are required [10], typically the dc currents are only injected briefly after relatively long time intervals; thus, their effect on performance (machine temperature, drive efficiency, etc.) can

This article has been accepted for inclusion in a future issue of this journal. Content is final as presented, with the exception of pagination.

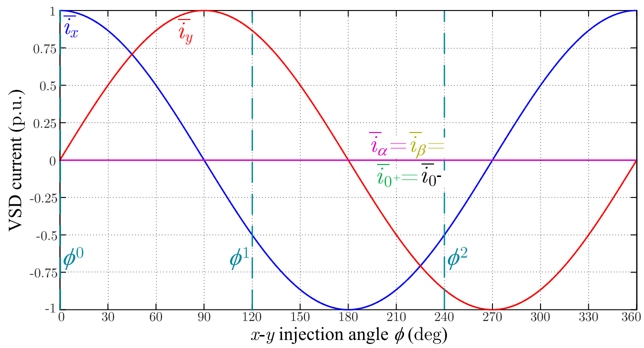

(a)

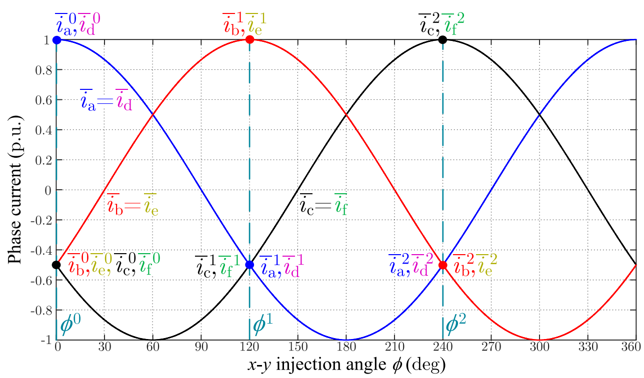

(b)

Fig. 2. Current dc components depending on the xy injection angle ϕ, for healthy drive. The ϕ applied by the proposed estimation method are ϕ^0, ϕ^1, and ϕ^2; the corresponding current values are indicated by solid circles. (a) VSD currents. (b) Phase currents.

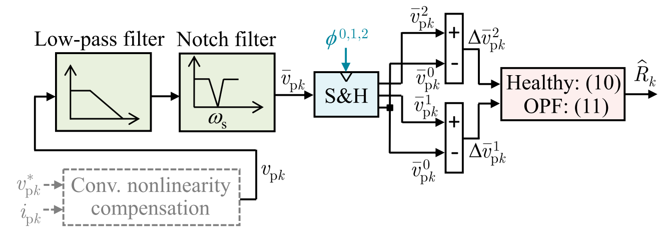

Fig. 3. Estimation of per-phase resistances from the pole voltages.

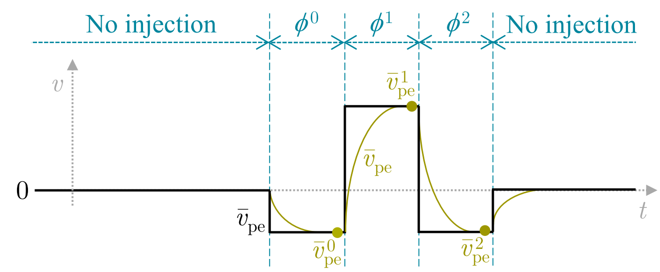

Fig. 4. Time sequence of dc injection and $\bar{v}_{pk}$ sampling (solid circles) to extract $\bar{v}_{pk}^\rho$, illustrated for phase e in healthy case.

be disregarded [15]. Concerning dc-link utilization, it is determined by the peak of the line voltages between pairs of phases whose back-electromotive forces are in opposition ($v_a - v_d$, $v_b - v_e$, or $v_c - v_f$) [31]; from Fig. 2(b), the corresponding pairs of dc phase currents are identical ($\bar{i}_a = \bar{i}_d$, $\bar{i}_b = \bar{i}_e$, and $\bar{i}_c = \bar{i}_f$), and hence those dc line voltages ($\bar{v}_a - \bar{v}_d$, $\bar{v}_b - \bar{v}_e$, and $\bar{v}_c - \bar{v}_f$) are expected to be relatively small and to normally have a negligible effect on the dc-link utilization.

The resistance estimation from the injected dc is addressed next. In phase k, the dc voltage and current are related as

$$\bar{v}_k^\rho = \left(\bar{i}_k^\rho - \bar{i}_{k\updownarrow}\right) R_k + \delta_k^\rho \tag{7}$$

where R_k represents phase-k stator resistance, δ_k^ρ denotes certain random uncertainty (e.g., measurement noise), and $\rho = 0$, 1, or 2 corresponds to the three injection angles [Fig. 2(b)]. The difference between $\bar{i}_k^\rho$ and $\bar{i}_{k\updownarrow}$ is that the former is the measured current value, and the latter is a measurement offset. Equation (7) may be rewritten so that it is expressed as a function of the pole voltage $\bar{v}_{pk}^\rho$ instead of the phase voltage

$$\bar{v}_{pk}^\rho = \left(\bar{i}_k^\rho - \bar{i}_{k\updownarrow}\right) R_k + \bar{v}_n^\rho + \delta_k^\rho \tag{8}$$

where $\bar{v}_n$ is the voltage between the stator neutral point and the dc-link midpoint, which is not zero in case of resistance asymmetry [12]. Assuming that $\bar{i}_{k\updownarrow}$ does not change fast, it can be canceled by subtracting the values in (8) at $\rho = 0$ from those at $\rho = 1$ or $\rho = 2$ (at close instants), giving

$$\Delta\bar{v}_{pk}^\rho = \Delta\bar{i}_k^\rho R_k + \Delta\bar{v}_n^\rho + \Delta\delta_k^\rho \tag{9}$$

where $\Delta\bar{u}^\rho = \bar{u}^\rho - \bar{u}^0$, with u being any signal and $\rho = 1, 2$.

Among the variables in (9), many of them are known. On the one hand, it can be assumed that the closed-loop current controller (Fig. 1) ensures effective tracking and hence $\Delta\bar{i}_k^\rho$ may be obtained from the current-reference values $\bar{i}_k^\rho$ indicated in Fig. 2. On the other hand, concerning $\Delta\bar{v}_{pk}^\rho$, to avoid extra passive filters and sensors for voltage measurements [12], [14], the pole voltages v_{pk} may be estimated from the pole-voltage references sent to the PWM module [15], [17], as shown at the bottom-left corner of Fig. 3. To this end, the dc voltage due to converter nonlinearities (dead time, turn-on/off delays, etc.) can be compensated for each phase as discussed in [15]. Otherwise, if it is desired to avoid potential inaccuracies of this compensation (e.g., for devices with relatively large and uncertain voltage drop), v_{pk} measurements [12] may be used for the proposal. Then, in either case, the ac components of v_{pk} are filtered out to obtain the dc components $\bar{v}_{pk}$. This is achieved by cascaded low-pass and notch digital filters [14], [17], as depicted in Fig. 3, where ω_s is the fundamental stator frequency. Subsequently, these values $\bar{v}_{pk}^\rho$ for each ϕ^ρ are extracted by a sample-and-hold (S & H) block. As shown in Fig. 4 for phase e, the $\bar{v}_{pk}^\rho$ values are taken at the end of each injection interval, after the $\bar{v}_{pk}$ exponential transient of the filters. Then, $\Delta\bar{v}_{pk}^\rho$ are computed based on $\bar{v}_{pk}^\rho$ (Fig. 3), so that they can be used for the resistance estimation.

Thus, ignoring uncertainty $\Delta\delta_k^\rho$, eight unknowns remain in (9): six R_k ($k = \mathrm{a}, \ldots, \mathrm{f}$) and two $\Delta\bar{v}_n^\rho$ ($\rho = 1, 2$) terms. From the twelve (six for $\rho = 1$ and six for $\rho = 2$) equations in (9), it is possible to form multiple combinations that have eight linearly independent equations so that the eight unknowns may be found. To select one of these combinations, the following procedure is applied using numerical simulation in Matlab: for each set of equations, the mean squared error between the actual R_k (balanced) and the calculated $\hat{R}_k$ (from $\Delta\bar{i}_k^\rho$ and $\Delta\bar{v}_{\mathrm{p}k}^\rho$, ignoring $\Delta\delta_k^\rho$) is computed for 10^6 sets of $\Delta\delta_k^\rho$ random values, and a combination of equations with low error is then chosen. Namely, the selected equations are those in (9) corresponding to $k=\mathrm{b,e,f}$ for $\rho=1$ and $k=\mathrm{a,c,d,e,f}$ for $\rho=2$. Solving this linear system of eight equations and eight unknowns, while considering $\Delta\delta_k^\rho=0$ and symbolic $\Delta\bar{v}_k^\rho$ and I_{dc}, yields the resistance estimates

$$\begin{bmatrix}\widehat{R}_{\mathrm{a}}\\ \widehat{R}_{\mathrm{b}}\\ \widehat{R}_{\mathrm{c}}\\ \widehat{R}_{\mathrm{d}}\\ \widehat{R}_{\mathrm{e}}\\ \widehat{R}_{\mathrm{f}}\end{bmatrix}=\frac{0.\widehat{6}}{I_{\mathrm{dc}}}\begin{bmatrix}0&0&0&-1&0&0&1&0\\ 1&0&-1&0&0&0&0&0\\ 0&0&0&0&1&0&-1&0\\ 0&0&0&0&0&-1&1&0\\ 0&1&-1&0&0&0&0&0\\ 0&0&0&0&0&0&-1&1\end{bmatrix}\begin{bmatrix}\Delta\bar{v}_{\mathrm{pb}}^1\\ \Delta\bar{v}_{\mathrm{pe}}^1\\ \Delta\bar{v}_{\mathrm{pf}}^1\\ \Delta\bar{v}_{\mathrm{pa}}^2\\ \Delta\bar{v}_{\mathrm{pc}}^2\\ \Delta\bar{v}_{\mathrm{pd}}^2\\ \Delta\bar{v}_{\mathrm{pe}}^2\\ \Delta\bar{v}_{\mathrm{pf}}^2\end{bmatrix}. \tag{10}$$

This novel formula is used in Fig. 3 to get $\widehat{R}_k$ in healthy case.

IV. DC Injection and R_k Estimation Under an OPF

In the following, an OPF is considered in phase a. Due to symmetry, the analysis is valid for OPFs in other phases, by simply applying a suitable rotation [17]. The fault constraint introduced in $\boldsymbol{A}$ by replacing in (4) its last row with the first row (for phase-a OPF) of $\boldsymbol{D}^{-1}$ (Section II-B) modifies the current distribution for given I_{dc} and ϕ. Namely, a i_{0^-} component arises, and the phase currents change accordingly, as shown in Fig. 5. It was proposed in [17] to use $\phi=90°$ and $\phi=270°=-90°$ to estimate the overall stator resistance, because these angles ensure $i_{0^-}=0$ [Fig. 5(a)] and hence minimum SCL, braking torque, and peak current. However, these choices are not suitable for estimating all R_k, because $\bar{i}_{\mathrm{d}}=0$ [Fig. 5(b)], making it difficult to obtain R_{d}. Furthermore, more than two ϕ should be applied to provide enough equations to solve for all the unknowns, similar to the healthy case (Section III). Instead, it is proposed here to use $\phi^0=103.9°$, $\phi^1=256.1°$, and $\phi^2=283.9°$. These are selected because they provide very small i_{0^-} [Fig. 5(a)], and significant current in all phases [Fig. 5(b)]: between 0.48 p.u. and 1.20 p.u. The small i_{0^-} yields an acceptable increase due to dc injection in terms of peak phase current (1.2 p.u.), SCL (1.12 p.u., normalized by $3I_{\mathrm{dc}}^2R$), and braking torque (−0.06 p.u., normalized by its maximum, for $\phi=0$). In fact, these values of increase, obtained for ϕ^0, ϕ^1, and ϕ^2 as explained in [17], are similar to those (minimum) found for $\phi=90°$ and $\phi=270°$ in [17]: 0.87 p.u., 1.0 p.u., and 0 p.u., respectively. They are also much lower than those for other ϕ values with larger i_{0^-} such as $\phi=0°$[17]: 2.0 p.u., 3.0 p.u., and −1.0 p.u., respectively. It may also be noticed in Fig. 5(b) that, for the selected angles ϕ^0, ϕ^1, and ϕ^2, the dc currents of the healthy phases with opposite back-electromotive forces (whose voltages determine the dc-link utilization [31]) are relatively

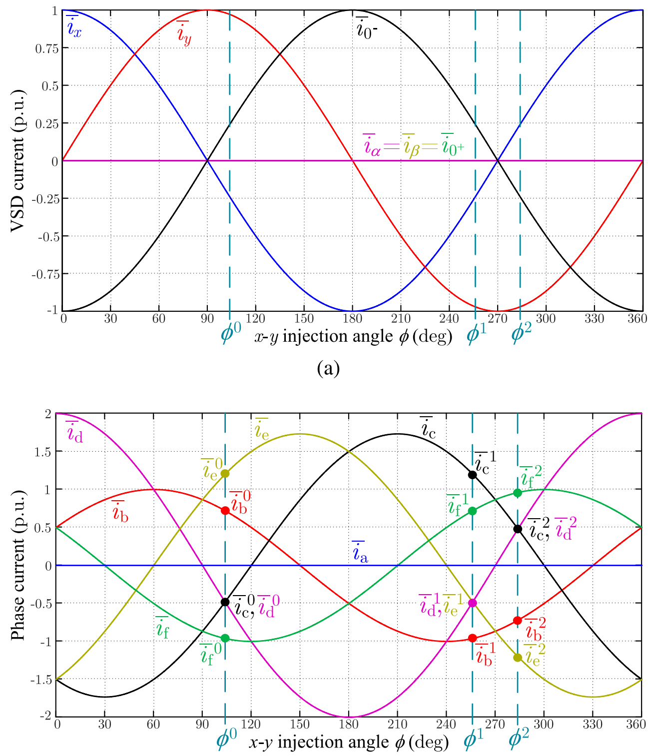

Fig. 5. Current dc components depending on the xy injection angle ϕ, for OPF in phase a. The ϕ applied by the proposed estimation method are ϕ^0, ϕ^1, and ϕ^2; the corresponding current values are indicated by solid circles. (a) VSD currents. (b) Phase currents.

similar pairwise ($|\bar{i}_{\mathrm{b}}-\bar{i}_{\mathrm{e}}|$ and $|\bar{i}_{\mathrm{c}}-\bar{i}_{\mathrm{f}}|$ give 0.48 p.u.); thus, the respective dc line voltages ($\bar{v}_{\mathrm{b}}-\bar{v}_{\mathrm{e}}$ and $\bar{v}_{\mathrm{c}}-\bar{v}_{\mathrm{f}}$) are expected to be even smaller than for other options such as $\phi=0°$ ($|\bar{i}_{\mathrm{b}}-\bar{i}_{\mathrm{e}}|=|\bar{i}_{\mathrm{c}}-\bar{i}_{\mathrm{f}}|=2$ p.u.).

Regarding the estimation under an OPF, (9) is still valid for all the phases k, except for the faulty one, which means that there are ten equations available. On the other hand, there are seven unknowns: five R_k ($k=\mathrm{b},\ldots,\mathrm{f}$) and two $\Delta\bar{v}_{\mathrm{n}}^\rho$ ($\rho=1,2$). Analogously to the healthy case, seven equations that yield low R_k mean squared error in the presence of uncertainty are selected after evaluation in Matlab: those corresponding to $k=\mathrm{b,c,d}$ for $\rho=1$ and $k=\mathrm{c,d,e,f}$ for $\rho=2$. Solving this linear system of seven equations and seven unknowns gives the following:

$$\begin{bmatrix}\widehat{R}_{\mathrm{b}}\\ \widehat{R}_{\mathrm{c}}\\ \widehat{R}_{\mathrm{d}}\\ \widehat{R}_{\mathrm{e}}\\ \widehat{R}_{\mathrm{f}}\end{bmatrix}=\frac{1}{I_{\mathrm{dc}}}\begin{bmatrix}-c_1&0&c_1&0&0&0&0\\ 0&c_1&-c_1&0&0&0&0\\ 0&c_2&-c_2&-c_3&c_3&0&0\\ 0&-c_4&c_4&c_5&0&-c_5&0\\ 0&c_6&-c_6&-c_7&0&c_7&0\end{bmatrix}\begin{bmatrix}\Delta\bar{v}_{\mathrm{pb}}^1\\ \Delta\bar{v}_{\mathrm{pc}}^1\\ \Delta\bar{v}_{\mathrm{pd}}^1\\ \Delta\bar{v}_{\mathrm{pc}}^2\\ \Delta\bar{v}_{\mathrm{pd}}^2\\ \Delta\bar{v}_{\mathrm{pe}}^2\\ \Delta\bar{v}_{\mathrm{pf}}^2\end{bmatrix};$$

$$\begin{aligned}&c_1=0.59476714;\ c_2=0.59460248;\ c_3=1.0406778\\ &c_4=0.23786733;\ c_5=0.41631724;\ c_6=0.2973424\\ &c_7=0.52041096.\end{aligned} \tag{11}$$

This novel formula is employed in Fig. 3 for the OPF case.

This article has been accepted for inclusion in a future issue of this journal. Content is final as presented, with the exception of pagination.

V. Experimental Results

The experimental tests are carried out with a symmetrical 6P induction motor (the same as in [11] and [17]) with a single neutral point. It has a four-pole 24-slot double-layer stator winding, with identical layout to that shown in [26] but fully pitched. The machine ratings are 2.8 A, 110 V, 1.1 kW, 7.5 Nm, 50 Hz, and 1400 $\mathrm{r/min}$. The stator resistance, obtained by using a multimeter at standstill in a certain phase, is 4.4 Ω. In the $\alpha\beta$ plane, the rotor resistance is 2.9 Ω, the stator and rotor leakage inductances are 10 mH and 21 mH, respectively, and the magnetizing inductance is 284 mH. The xy stator leakage inductance, obtained according to [26], is 4.52 mH. For the zero sequence 0^-, the rotor resistance, rotor leakage inductance, and magnetizing inductance associated with the third-order space harmonic for 2-A dc excitation are 3.5 Ω, 20.4 mH, and 50.2 mH, respectively [17].

A photo of the experimental setup may be found in [11, Fig. 6]. The 6P motor is coupled to a dc generator, loaded by a variable resistor. The motor is driven by a pair of three-phase IKCM30F60GD inverters, with dc-link voltage kept at 300 V by a GEN-300-11-3P480 dc supply. The dc-link capacitance is 3.3 mF. The control and estimation algorithms are implemented in a dSPACE-MicroLabBox-1202 platform. The analog-to-digital converters have 16 bits. The current control is designed as explained in Section II-C, including an outer proportional-integral speed controller based on indirect rotor field-oriented control [27]. The ac current references in the secondary subspaces are set to zero in healthy conditions and follow the ML strategy under OPF [4], [6], [8], [30]. For the dc-voltage extraction needed for the estimation (Fig. 3), the low-pass filter is obtained by cascading two first-order low-pass filters with bandwidth of 7 rad/s, and the notch filter is a second-order one with quality factor of 0.5. For each of the estimation instances, the duration of each of the three consecutive injection intervals (Fig. 4) is set to 2 s. The sampling and switching frequency is 10 kHz. Four adjustable resistors are used to emulate resistance asymmetry [11].

A Matlab/Simulink implementation of the proposed method, including the parameter values used in most of the experimental tests, is available for download as supplementary material in this article.

A. Proposed Method at Certain Operating Conditions

1) Per-Phase Resistance Estimates: The method is first tested, using $I_{\mathrm{dc}} = 2$ A at 500 $\mathrm{r/min}$, in four different scenarios, namely healthy conditions with or without external resistors and phase-a OPF with or without external resistors. The load of the dc generator is adjusted between healthy and faulty conditions so that in both cases the highest rms phase current in steady state is equal to rated; this happens for $\alpha\beta$ current modulus of $|i_{\alpha\beta}| = 3.96$ A and $|i_{\alpha\beta}| = 2.75$ A, respectively. The pole voltages are estimated from their references (Fig. 3). When the extra resistors are included, they are connected in series with the stator phases a, b, c, and d. The resistance R_k of each stator phase is estimated online ($\widehat{R}_k$) using the proposal at four consecutive instances for each of the four tested scenarios within a total operation time of roughly 15 min. In addition, R_k are measured offline at standstill, before and after the online tests, by applying a dc current of 2 A to each phase by a dc source and dividing the measured dc voltage and current. All the resulting online-estimated $\widehat{R}_k$ and offline-measured R_k are displayed, with a resolution of 0.01 Ω and 0.05 Ω, respectively, in Tables II–V, one table per scenario. The extra resistances are relatively large, so that they may represent demanding situations such as high-resistance connections [10]. There is a certain resistance increase throughout the process due to normal temperature rise during operation. Most importantly, from these tables, the proposal provides a good accuracy and precision,

TABLE II
Measured R_k and Estimated $\widehat{R}_k$ (Ω) in Healthy Conditions Without External Resistors

Phase	Measured offline beforehand	Novel online estimation				Measured offline afterward
		1st	2nd	3rd	4th	
a	4.50	4.46	4.53	4.56	4.60	4.60
b	4.40	4.36	4.43	4.45	4.48	4.50
c	4.45	4.45	4.52	4.54	4.57	4.60
d	4.40	4.43	4.50	4.52	4.56	4.50
e	4.35	4.33	4.40	4.43	4.46	4.50
f	4.40	4.46	4.53	4.55	4.58	4.45

TABLE III
Measured R_k and Estimated $\widehat{R}_k$ (Ω) in Healthy Conditions With External Resistors

Phase	Measured offline beforehand	Novel online estimation				Measured offline afterward
		1st	2nd	3rd	4th	
a	7.50	7.43	7.49	7.52	7.53	7.60
b	9.40	9.44	9.50	9.53	9.53	9.60
c	6.50	6.54	6.61	6.63	6.64	6.65
d	8.80	8.81	8.86	8.80	8.81	8.85
e	4.55	4.55	4.61	4.64	4.64	4.60
f	4.45	4.52	4.58	4.61	4.60	4.50

TABLE IV
Measured R_k and Estimated $\widehat{R}_k$ (Ω) Under Phase a Open Without External Resistors

Phase	Measured offline beforehand	Novel online estimation				Measured offline afterward
		1st	2nd	3rd	4th	
b	4.25	4.24	4.32	4.35	4.35	4.35
c	4.40	4.27	4.38	4.38	4.40	4.50
d	4.40	4.34	4.37	4.37	4.38	4.45
e	4.30	4.26	4.38	4.38	4.40	4.35
f	4.35	4.30	4.39	4.39	4.41	4.45

TABLE V
Measured R_k and Estimated $\widehat{R}_k$ (Ω) Under Phase a Open With External Resistors

Phase	Measured offline beforehand	Novel online estimation				Measured offline afterward
		1st	2nd	3rd	4th	
b	9.45	9.50	9.44	9.45	9.46	9.50
c	6.60	6.48	6.44	6.49	6.49	6.60
d	8.80	8.84	8.81	8.84	8.83	8.90
e	4.50	4.31	4.29	4.31	4.31	4.55
f	4.40	4.51	4.50	4.53	4.52	4.50

This article has been accepted for inclusion in a future issue of this journal. Content is final as presented, with the exception of pagination.

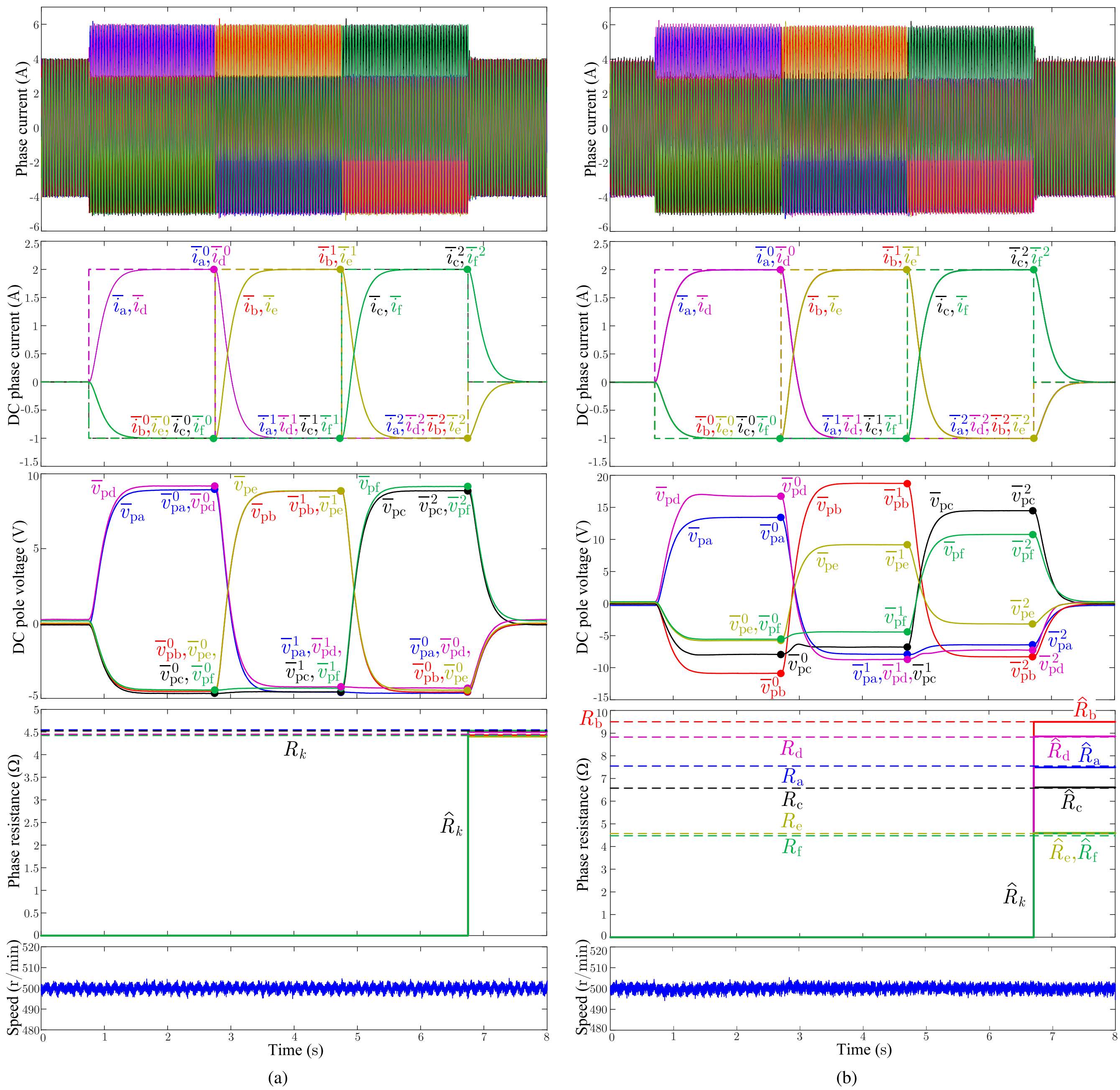

Fig. 6. Experimental waveforms of the proposed method in healthy conditions. (a) Without external resistors. (b) With external resistors.

i.e., the estimates $\widehat{R}_k$ for the four different instances of the same scenario (table) and phase (row) are close to each other and also close to the respective offline measurements R_k.

2) Waveforms: The main signals obtained for the second online estimation from each of the Tables II–V are shown in Figs. 6(a), 6(b), 7(a), and 7(b), respectively. The correspondence between phases and colors is the same as in Figs. 2(b) and 5(b). The dc currents are extracted from the phase currents by applying filters identical to those used for the voltages (Fig. 3). These dc current values (solid) are not employed for calculating the resistance estimates because during the R_k estimation, they are assumed to match the predefined dc current references (dashed), as justified in Section III; nevertheless, they are displayed to prove that this assumption is valid, thanks to the effective current control from Fig. 2. Note that the dc current references for the three consecutive injection angles in Figs. 6 and 7 match the values theoretically defined in Figs. 2(b) and 5(b), respectively, simply multiplied by $I_{\mathrm{dc}} = 2$ A. Although the currents are practically equal regardless of whether there is resistance asymmetry (right) or not (left), the dc pole voltages extracted (sampled at the solid circles) using the proposed scheme from Fig. 3 vary to a substantial extent,

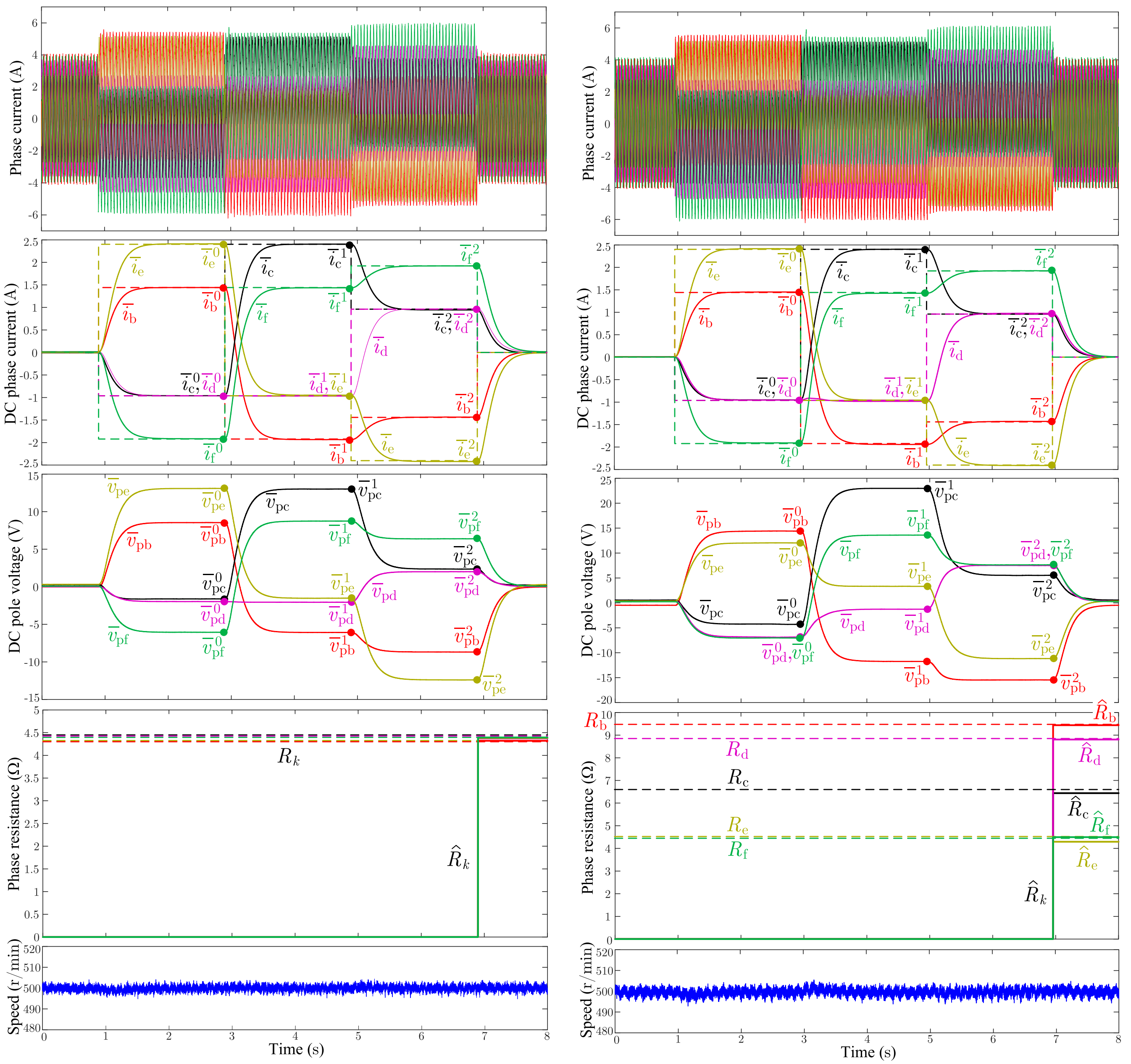

(a) (b)

Fig. 7. Experimental waveforms of the proposed method under phase a open. (a) Without external resistors. (b) With external resistors.

yielding different resistance estimates $\widehat{R}_k$. In agreement with the tables, the $\widehat{R}_k$ signals (solid) are very close to the respective actual R_k values (dashed), the latter of which are found by interpolation between the resistances measured offline at the beginning and end of the test of each scenario. Additionally, it is worth highlighting that the speed is not altered noticeably by the dc injection, because it does not introduce any relevant torque disturbances.

3) Secondary Effects: For the injection angles of the proposed method, several figures of merit about the impact of the dc injection on the drive performance are displayed in Tables VI and VII for healthy and OPF conditions, respectively. These values are also compared with those without injection and those for $\phi = 0°$ and $\phi = 90°$ [17],[1] which for OPF represents an unfavorable case ($\phi = 0°$) and the choice ($\phi = 90°$) in [17] to estimate the overall (not per-phase) stator resistance. For OPF, $\phi = 60°$ [$\bar{i}_{\mathrm{e}} = 0$ in Fig. 5(b)] is also compared, which would be needed in addition to $\phi = 90°$ ($\bar{i}_{\mathrm{d}} = 0$) if it is attempted to adapt the method from [12] (which nullifies two healthy $\bar{i}_k$ consecutively) to an OPF. It can be observed in Tables VI and VII that the increase values in peak current and SCL are moderate for the ϕ angles used with the proposal

[1]In Table VI, the case $\phi = 0°$ would match ϕ^0 [$\phi^0 = 0°$ in Fig. 2(b)].

TABLE VI
PEAK PHASE CURRENT, SCL, TORQUE/SPEED DISTURBANCE AND DROP IN DC-LINK UTILIZATION IN HEALTHY CONDITIONS, FOR $I_{dc} = 2$ A

	No external resistors					With external resistors				
	No injection	$\phi = 90°$	Proposed			No injection	$\phi = 90°$	Proposed		
			ϕ^0	ϕ^1	ϕ^2			ϕ^0	ϕ^1	ϕ^2
Peak phase current (A)	4.0	5.7	6.0	6.0	6.0	4.0	5.7	6.0	6.0	6.0
Max. dc phase current (A)	0	1.7	2.0	2.0	2.0	0	1.7	2.0	2.0	2.0
SCL (W)	207	259	260	260	260	310	376	407	398	382
Speed change (r/min)	–	≈ 0	≈ 0	≈ 0	≈ 0	–	≈ 0	≈ 0	≈ 0	≈ 0
Drop in dc-link utilization (V)	–	0.1	0.3	0.3	0.3	–	8.6	5.1	9.6	5.1

TABLE VII
PEAK PHASE CURRENT, SCL, TORQUE/SPEED DISTURBANCE AND DROP IN DC-LINK UTILIZATION UNDER PHASE a OPEN, FOR $I_{dc} = 2$ A

	No external resistors							With external resistors						
	No injection	$\phi = 0°$†	$\phi = 60°$‡	$\phi = 90°$†	Proposed			No injection	$\phi = 0°$†	$\phi = 60°$‡	$\phi = 90°$†	Proposed		
					ϕ^0	ϕ^1	ϕ^2					ϕ^0	ϕ^1	ϕ^2
Peak phase current (A)	4.0	8.0	6.3	5.7	6.0	6.0	6.0	4.0	8.0	6.3	5.7	6.0	6.0	6.0
Max. dc phase current (A)	0	4.0	3	1.7	2.4	2.4	2.4	0	4.0	3	1.7	2.4	2.4	2.4
SCL (W)	127	295	208	180	188	188	185	211	487	356	285	289	307	288
Speed change (r/min)	–	20	7	≈ 0	≈ 0	≈ 0	≈ 0	–	20	7	≈ 0	≈ 0	≈ 0	≈ 0
Drop in dc-link utilization (V)	–	19.3	8.3	0.1	4.5	4.6	4.0	–	25.4	17.8	8.4	2.8	15.1	4.3

† $\phi = 90°$ [17] (unsuitable for R_k estimation) and $\phi = 0°$ correspond to the most beneficial and detrimental ϕ values, respectively, regarding peak phase current, SCL and torque/speed disturbance under an OPF (see Section IV).
‡ $\phi = 60°$ corresponds to nullifying a healthy dc phase current, analogously to what is done in [12] for healthy case.

(ϕ^0, ϕ^1, ϕ^2), close to those with $\phi = 90°$ [17], and lower (for OPF) than those for $\phi = 60°$ and (especially) $\phi = 0°$. Actually, although the maximum $\bar{i}_k$ under OPF (Table VII) is notably greater for the adopted angles (2.4 A) than for $\phi = 90°$ (1.7 A), this is counteracted to a great extent by the fact that the highest dc increase occurs in the phases c and e [Fig. 5(b)], which for the ML fault-tolerant strategy has lower ac current [17, Fig. 9(b)]. This is why the peak current is nearly the same for ϕ^0, ϕ^1, ϕ^2 and $\phi = 90°$ in Table VII. On the other hand, a transient speed change when the dc injection is applied (see, e.g., [17, Fig. 13]) would reflect any braking torque caused by the dc [17]. From Tables VI and VII, this is negligible for all the considered ϕ except $\phi = 0°$ and $\phi = 60°$ for OPF, which are not part of the proposal. Concerning the drop in dc-link utilization, it is calculated as the dc line voltage between the healthy phases with opposite back-electromotive forces, as aforementioned. In the most unfavorable scenario for the proposal (Table VII and cf. Fig. 7), it is 15.1 V; this is just 4.8% of the maximum line voltage without dc injection $2\sqrt{2} \cdot 110$ V in spite of the large resistance imbalance.

In summary, per-phase resistance estimation is achieved by the proposed technique in either healthy or OPF situation, with a relatively low drop in dc-link utilization and increase in peak current, SCL and torque/speed disturbance, even if the resistance asymmetry is substantial. Compared with the existing literature (Table I), it is the first time that this has been accomplished. Furthermore, it is here done without using additional devices such as voltage sensors.

4) Estimation Root-Mean-Square Error (RMSE) With/Without Voltage Measurements: The estimation accuracy is further assessed quantitatively next, through the RMSE. For each of the four scenarios (same scenarios as in Tables II–V), the error of all $\widehat{R}_k$ at multiple instances (15 per case) is considered to yield a single RMSE value per scenario. This is done for the alternatives of using the voltage references or measured pole voltages for the estimation. For the latter, the dc is extracted from the analog voltages by second-order passive RC filters with bandwidth of 0.2 Hz. The actual resistances are measured offline before and after the online estimations, as for Tables II–V, and interpolation between them is performed to obtain the actual resistances R_k for each of the online estimation instances. The resulting RMSEs are displayed in Table VIII. The RMSEs are similarly low when using voltage sensors compared to when not using them, although slightly smaller in some cases. For both approaches, the RMSE is small, confirming the good accuracy. In any case, great accuracy is often not needed; e.g., for high-resistance connections, R_k tends to rise indefinitely until detected [10].

TABLE VIII
ESTIMATION RMSE FOR 500 r/min AND $I_{dc} = 2$ A

	Healthy		OPF	
With/without external resistors?	Without	With	Without	With
RMSE (Ω) without voltage sensors	0.347	0.305	0.205	0.228
RMSE (Ω) with voltage sensors	0.135	0.151	0.092	0.240

B. Proposed Method at Other Conditions

1) Small Injected DC Current: I_{dc} was set relatively large (2 A), so it was a particularly unfavorable case when assessing the potential detrimental effects in Tables VI and VII. Nevertheless, if I_{dc} is decreased (e.g., to reduce even more those

This article has been accepted for inclusion in a future issue of this journal. Content is final as presented, with the exception of pagination.

TABLE IX
ESTIMATION RMSE FOR 500 r/min, OPF, EXTERNAL RESISTORS, AND VARIABLE I_{dc}

I_{dc} (A)	0.2	0.4	1	2
RMSE (Ω) without voltage sensors	0.481	0.249	0.244	0.228
RMSE (Ω) with voltage sensors	0.324	0.186	0.228	0.240

TABLE X
ESTIMATION RMSE FOR OPF, EXTERNAL RESISTORS, WITH $I_{\mathrm{dc}} = 2$ A, AND VARIOUS LOADS AND SPEEDS

Speed (r/min)	500		1100	
$\lvert i_{\alpha\beta}\rvert$ (A)	1.58	2.75	1.58	2.75
RMSE (Ω) without voltage sensors	0.176	0.228	0.161	0.408
RMSE (Ω) with voltage sensors	0.256	0.240	0.218	0.316

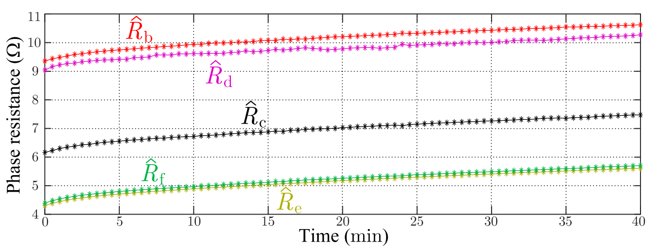

Fig. 8. Resistance estimates of the proposed method for a prolonged time under phase a open and with external resistors.

effects), then the RMSE is still low, as reflected in Table IX for an OPF with extra resistors. The RMSE only worsens noticeably when I_{dc} is made really small, such as 0.2 A. $I_{\mathrm{dc}} = 0.4$ A could be adopted with good accuracy.

2) Other Loads and Speeds: The RMSE of the proposal is shown for other speeds and loads in Table X. Changing the speed and load also implies varying other parameters such as inductances and flux. From Table X, a reasonable accuracy is also obtained at different operating conditions.

3) Temperature Increase: Fig. 8 depicts the evolution of $\widehat{R}_k$, estimated every 30 s, for a long operation time, 500 r/min, OPF, $|i_{\alpha\beta}| = 2.75$ A, and with extra resistors (as a worst-case imbalance scenario). During this period, the motor is driven with operating conditions as in Fig. 7(b). From Fig. 8, $\widehat{R}_k$ increase with time by more than 1 Ω due to the machine heating as it could be expected, illustrating the method suitability to reflect and monitor the effect of temperature.

C. Comparison with the Method from [17]

The resistance estimation method from [17] for OPF, which assumed balanced R_k, is also tested here under an OPF. The resulting RMSE is 0.221 Ω without external resistors, and 2.19 Ω when adding the same resistors as in Table V. The latter RMSE is much greater than for the proposal (0.228 Ω or 0.240 Ω; Table VIII), due to the fact that this previous method [17] is not able to provide different $\widehat{R}_k$ for each phase.

VI. CONCLUSION

This article has proposed a technique based on dc injection for estimating the per-phase stator resistances in 6P induction machines with symmetrical winding arrangement and a single neutral point, either in healthy or OPF conditions. The main novelty and research contribution with respect to related available publications is the ability of the method to estimate, for the first time, the per-phase resistances under an OPF. It is designed so that the estimation can be performed from the pole-voltage references without extra measurements or devices, or from measured pole voltages (for even better accuracy), in spite of the neutral-point voltage deviation due to resistance asymmetries. The dc current, injected periodically, is distributed among the phases so that there is no torque ripple (no $\alpha\beta$ dc current) and so that (by ϕ choice) the increase in loss, braking torque, and peak current is relatively small. The theory is validated by experimental tests, performed at several operating conditions. Future work may extend the method and analysis for other drive topologies or further improve the robustness to uncertainties.

REFERENCES

[1] A. G. Yepes, O. Lopez, I. Gonzalez-Prieto, M. Duran, and J. Doval-Gandoy, "A comprehensive survey on fault tolerance in multiphase AC drives, Part 1: General overview considering multiple fault types," *Machines*, vol. 10, no. 3, 2022, Art. no. 208.

[2] W. Taha, P. Azerb, A. D. Callegaro, and A. Emadi, "Multiphase traction inverters: State-of-the-art review and future trends," *IEEE Access*, vol. 10, pp. 4580–4599, 2022.

[3] E. Levi, "Multiphase electric machines for variable-speed applications," *IEEE Trans. Ind. Electron.*, vol. 55, no. 5, pp. 1893–1909, May 2008.

[4] M. Duran and F. Barrero, "Recent advances in the design, modeling and control of multiphase machines—Part 2," *IEEE Trans. Ind. Electron.*, vol. 63, no. 1, pp. 459–468, Jan. 2016.

[5] G. Sala, M. Mengoni, G. Rizzoli, M. Degano, L. Zarri, and A. Tani, "Impact of star connection layouts on the control of multiphase induction motor drives under open-phase fault," *IEEE Trans. Power Electron.*, vol. 36, no. 4, pp. 3717–3726, Apr. 2021.

[6] W. N. W. A. Munim, M. J. Duran, H. S. Che, M. Bermúdez, I. Gonzalez-Prieto, and N. A. Rahim, "A unified analysis of the fault tolerance capability in six-phase induction motor drives," *IEEE Trans. Power Electron.*, vol. 32, no. 10, pp. 7824–7836, Oct. 2017.

[7] W. Zhang, D. Xu, P. N. Enjeti, H. Li, J. T. Hawke, and H. S. Krishnamoorthy, "Survey on fault-tolerant techniques for power electronic converters," *IEEE Trans. Power Electron.*, vol. 29, no. 12, pp. 6319–6331, Dec. 2014.

[8] A. G. Yepes, I. Gonzalez-Prieto, O. Lopez, M. Duran, and J. Doval-Gandoy, "A comprehensive survey on fault tolerance in multiphase AC drives, Part 2: Phase and switch open-circuit faults," *Machines*, vol. 10, no. 3, 2022, Art. no. 221.

[9] A. Gonzalez-Prieto, I. Gonzalez-Prieto, A. G. Yepes, M. J. Duran, and J. Doval-Gandoy, "On the advantages of symmetrical over asymmetrical multiphase AC drives with even phase number using direct controllers," *IEEE Trans. Ind. Electron.*, vol. 69, no. 8, pp. 7639–7650, Aug. 2022.

[10] L. Zarri et al., "Detection and localization of stator resistance dissymmetry based on multiple reference frame controllers in multiphase induction motor drives," *IEEE Trans. Ind. Electron.*, vol. 60, no. 8, pp. 3506–3518, Aug. 2013.

[11] A. G. Yepes et al., "Online control strategy for tolerating resistance asymmetry with minimum copper loss in the full torque range for symmetrical six-phase AC drives," *IEEE Trans. Power Electron.*, vol. 38, no. 1, pp. 151–164, Jan. 2023.

[12] J. Sun, C. Li, Z. Zheng, K. Wang, and Y. Li, "Online estimation of per-phase stator resistance based on DC-signal injection for condition monitoring in multiphase drives," *IEEE Trans. Ind. Electron.*, vol. 69, no. 3, pp. 2227–2239, Mar. 2022.

[13] P. Zhang, Y. Du, T. G. Habetler, and B. Lu, "A survey of condition monitoring and protection methods for medium-voltage induction motors," *IEEE Trans. Ind. Appl.*, vol. 47, no. 1, pp. 34–46, Jan./Feb. 2011.

[14] F. Baneira, A. G. Yepes, O. Lopez, and J. Doval-Gandoy, "Estimation method of stator winding temperature for dual three-phase machines based on DC-signal injection," *IEEE Trans. Power Electron.*, vol. 31, no. 7, pp. 5141–5148, Jul. 2016.

[15] S. Cheng, Y. Du, J. A. Restrepo, P. Zhang, and T. G. Habetler, "A nonintrusive thermal monitoring method for induction motors fed by closed-loop inverter drives," *IEEE Trans. Power Electron.*, vol. 27, no. 9, pp. 4122–4131, Sep. 2012.

[16] Z. Li, G. Feng, C. Lai, W. Li, and N. C. Kar, "Current injection-based simultaneous stator winding and PM temperature estimation for dual three-phase PMSMs," *IEEE Trans. Ind. Appl.*, vol. 57, no. 5, pp. 4933–4945, Sep./Oct. 2021.

[17] A. G. Yepes, M. S. Abdel-Majeed, H. S. Che, A. S. Abdel-Khalik, S. Ahmed, and J. Doval-Gandoy, "DC-signal injection for stator-resistance estimation in symmetrical six-phase induction motors under open-phase fault," *IEEE Trans. Ind. Electron.*, vol. 70, no. 6, pp. 5444–5453, Jun. 2023.

[18] M. M. Swamy, T. Kume, Y. Yukihira, S. Fujii, and M. Sawamura, "A novel stopping method for induction motors operating from variable frequency drives," *IEEE Trans. Power Electron.*, vol. 19, no. 4, pp. 1100–1107, Jul. 2004.

[19] F. Baneira, J. Doval-Gandoy, A. G. Yepes, and O. Lopez, "DC-current injection with minimum torque ripple in interior permanent-magnet synchronous motors," *IEEE Trans. Power Electron.*, vol. 35, no. 2, pp. 1176–1181, Feb. 2020.

[20] J. Yoo, J. Lee, S.-K. Sul, and N. A. Baloch, "Stator resistance estimation using DC injection with reduced torque ripple in induction motor sensorless drives," *IEEE Trans. Ind. Appl.*, vol. 56, no. 4, pp. 3744–3754, Jul./Aug. 2020.

[21] S. Ouenzerfi, H. Zahr, M. Trabelsi, E. Semail, S. Harmand, and R. Boubaker, "3-D multi-nodal thermal modelling for fault-tolerant machine," in *Proc. IEEE ICIT*, Feb. 2019, pp. 1551–1556.

[22] N. Bianchi, E. Fornasiero, and S. Bolognani, "Thermal analysis of a five-phase motor under faulty operations," *IEEE Trans. Ind. Appl.*, vol. 49, no. 4, pp. 1531–1538, Jul./Aug. 2013.

[23] M. Popescu, D. G. Dorrell, L. Alberti, N. Bianchi, D. A. Staton, and D. Hawkins, "Thermal analysis of duplex three-phase induction motor under fault operating conditions," *IEEE Trans. Ind. Appl.*, vol. 49, no. 4, pp. 1523–1530, Jul./Aug. 2013.

[24] Z. Kuang, S. Wu, B. Du, H. Xu, S. Cui, and C. C. Chan, "Thermal analysis of fifteen-phase permanent magnet synchronous motor under different fault tolerant operations," *IEEE Access*, vol. 7, pp. 81466–81480, 2019.

[25] K. Lee, L. Li, K. Bai, X. Ouyang, and H. Yang, "Harmonic model and remedy strategy of multiphase PM motor under open-circuit fault," *IEEE/ASME Trans. Mechatron.*, vol. 24, no. 3, pp. 1407–1419, Jun. 2019.

[26] A. S. Abdel-Khalik, M. S. Abdel-Majeed, and S. Ahmed, "Effect of winding configuration on six-phase induction machine parameters and performance," *IEEE Access*, vol. 8, pp. 223009–223020, 2020.

[27] E. Levi, "FOC: Field oriented control," in *The Industrial Electronics Handbook* in Power Electronics and Motor Drives, 2nd ed. Boca Raton, FL, USA: CRC Press, 2011.

[28] F. Baneira, J. Doval-Gandoy, A. G. Yepes, O. Lopez, and D. Perez-Estevez, "Control strategy for multiphase drives with minimum losses in the full torque operation range under single open-phase fault," *IEEE Trans. Power Electron.*, vol. 32, no. 8, pp. 6275–6285, Aug. 2017.

[29] M. Hu, W. Hua, Z. Wu, and Y. Hu, "Discrete-time current control of salient machines with a simplified model," *IEEE Trans. Ind. Electron.*, vol. 70, no. 7, pp. 6686–6698, Jul. 2023.

[30] H. S. Che, M. J. Duran, E. Levi, M. Jones, W.-P. Hew, and N. Abd Rahim, "Postfault operation of an asymmetrical six-phase induction machine with single and two isolated neutral points," *IEEE Trans. Power Electron.*, vol. 29, no. 10, pp. 5406–5416, Oct. 2014.

[31] A. G. Yepes, J. Doval-Gandoy, F. Baneira, and H. Toliyat, "Comparison of stator winding connections in multiphase drives under healthy operation and with one open converter leg," *IET Electric Power Appl.*, vol. 14, no. 4, pp. 584–596, Apr. 2020.

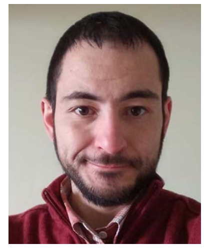

Alejandro G. Yepes (Senior Member, IEEE) received the M.Sc. and Ph.D. degrees in electrical engineering from the Universidade de Vigo, Vigo, Spain, in 2009 and 2011, respectively.

Since 2008, he has been with the Applied Power Electronics Technology Research Group, Universidade de Vigo. From 2016 to 2018, he was a Visiting Scholar with the Department of Electrical and Computer Engineering, Texas A&M University, College Station, TX, USA. His research interest includes electric machine drives.

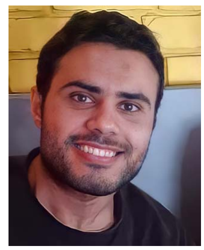

Mahmoud S. Abdel-Majeed received the B.Sc. degree in electrical engineering from Alexandria University, Alexandria, Egypt, in 2019.

He is currently a Researcher with the Faculty of Engineering, Alexandria University. His research interests include battery chargers, electric vehicles, smart grids, and power electronics.

Wessam E. Abdel-Azim received the B.Sc. degree in electrical engineering from Alexandria University, Alexandria, Egypt, in 2018.

He is currently a Teaching Assistant with the Department of Electrical, Faculty of Engineering, Alexandria University. His research interests include electric drives, power electronics, and pulsed power applications.

Mohamed G. Abdel-Moneim received the B.Sc. degree in electrical engineering from Alexandria University, Alexandria, Egypt, in 2021.

He is currently a Teaching Assistant with the Electrical Engineering Department, Faculty of Engineering, Alexandria University. His research interests include power electronics, battery chargers, electric drives, and electric vehicles.

Ayman Samy Abdel-Khalik (Senior Member, IEEE) received the B.Sc. and M.Sc. degrees from Alexandria University, Alexandria, Egypt, in 2001 and 2004, respectively, and the Ph.D. degree from Alexandria University and Strathclyde University, Glasgow, U.K., in 2009, under a dual channel program, all in electrical engineering.

He is currently a Professor with the Electrical Engineering Department, Faculty of Engineering, Alexandria University. His research interests include electrical machine design and modeling, electric drives, energy conversion, and renewable energy.

Dr. Abdel-Khalik serves as the Editor-in-Chief of *Alexandria Engineering Journal* and an Associate Editor of IEEE TRANSACTIONS ON INDUSTRIAL ELECTRONICS and *IET Electric Power Applications* Journal.

Shehab Ahmed (Senior Member, IEEE) received the B.Sc. degree in electrical engineering from Alexandria University, Alexandria, Egypt, in 1999, and the M.Sc. and Ph.D. degrees in electrical engineering from Texas A&M University, College Station, TX, USA, in 2000 and 2007, respectively.

He is currently a Professor and the Chair of the Electrical and Computer Engineering, CEMSE Division, King Abdullah University of Science and Technology, Thuwal, Saudi Arabia. He was with Schlumberger Technology Corporation, Houston, TX, from 2001 to 2007, developing downhole mechatronic systems for oilfield service products. He was with Texas A&M University at Qatar, Doha, Qatar, from 2007 to 2018. His research interests include subsurface mechatronics, solid-state power conversion, electric machines, and drives.

Jesús Doval-Gandoy (Member, IEEE) received the M.Sc. and Ph.D. degrees in electrical engineering from the Polytechnic University of Madrid, Madrid, Spain, and from Universidade de Vigo, Vigo, Spain, in 1991 and 1999, respectively.

He is a Professor and the Head of the Applied Power Electronics Technology Research Group (APET), Universidade de Vigo. His research interest includes the area of ac power conversion.